SAND2022-0513C

The number of total pages of the manuscript should be **2 pages**

Extended Summary template (for draft and final papers)

The 10th International Conference on Modeling and Diagnostics for Advanced Engine Systems (COMODIA 2022), July 5-8, 2022, Sapporo, Japan

Paper Number: 0045
Effects of Passive Pre-chamber Geometry and Ignition System on the Engine Performance

*Francesco Di Sabatino[1], Pablo Jose Martinez-Hernandiz[2], Ricardo Novella Rosa[2], Isaac Ekoto[1]

[1] *Combustion Research Facility, Sandia National Laboratories*
Livermore, CA, 94550, United States
[2] *CMT - Motores Térmicos, Universitat Politècnica de València*
Valencia, 46022, Spain

Key Words: Turbulent Jet Ignition; Non-equilibrium Plasma Discharges; Lean Combustion; Spark-ignited Engines; Advanced Ignition; OH* Chemiluminescence Imaging

INTRODUCTION

Lean combustion is a promising technology to reduce SI engines emissions and improve performance [1]–[3]. However, poor ignition stability has been highlighted as a drawback of this combustion mode [4]. Several techniques have been considered to improve the repeatability of ignition processes to include igniters that use non-equilibrium plasma discharges [5] as well as pre-chambers (PC) [6].

Pre-chamber ignition is characterized by generated jets of combustion products or active radicals that propagate from the pre-chamber into the main chamber, and serve as a distributed source of ignition. Passive PCs – without auxiliary fueling into the pre-chamber – have demonstrated effectiveness to enhance combustion stability [7], [8].

Passive pre-chamber engine combustion studies by Novella et al. [7] observed that lean and exhaust gas recirculation (EGR) limits strongly depended on PC geometry, as well as the ability to remove residual gases from the PC volume. Zhou et al. [8] concluded that an axially orientated nozzle could accelerate main-chamber combustion rates, improve engine performance, and reduce emissions at lean conditions. The authors of [7], [8] utilized a conventional inductive ignition coil/spark plug system to ignite the two chambers, while advanced igniters based on non-equilibrium plasma discharges have been demonstrated to be effective in increasing flame speed and improving the ignition process of SI engines [9], [10]. However, only a very recent study has shown the use of nanosecond repetitively pulsed (NRP) plasma discharges in a pre-chamber configuration [11]. Merotto et al. [11] highlighted that the ignition process and early flame propagation was enhanced by the NRP plasma discharges compared to the inductive ones, especially at lean conditions. Even though this study presented insightful and important information on the use of NRP plasma discharges in a pre-chamber configuration, the experimental campaign was performed in a constant volume vessel without the in- and out-flows present for an engine igniter. Therefore, it is of interest to investigate the use of NRP plasma discharges in passive pre-chambers connected to a SI engine.

The present work had two objectives. First, engine performance was evaluated for variations in pre-chamber geometry: namely smaller or larger volumes and pre-chamber tips with or without an axial hole nozzle. Second, engine performance with either a conventional inductive spark igniter or an NRP plasma ignition system was used for pre-chamber combustion initiation. Flame chemiluminescence images complemented apparent heat release rate (HRR) measurements and provided insight on cyclic stability mechanisms.

EXPERIMENTAL SETUP

The Sandia 4-stroke, optically-accessible single-cylinder research engine (SCRE) developed by General Motors (SG2) was used to perform the experimental campaign. Detailed characteristics of this engine were discussed in previous studies [12].

The engine features a 13:1 geometric compression ratio. A single fuel injection at 330 crank angles (CA) before top dead center (TDC) was used to generate a homogeneous fuel-air charge in the main chamber. The engine speed was kept constant at 1300 rotation per minute (rpm) using a motoring dynamometer connected to an optical encoder with 0.1 CA resolution to measure crank location. A research gasoline with an 87 anti-knock index (RD5-87) was used as the fuel. A piezo-electric pressure transducer (Kistler 6135A) installed in the engine head was used to measure in-cylinder pressure. Time-resolved (40 kHz) image sets of excited hydroxyl radical (OH*) chemiluminescence from main-chamber combustion were visualized through a piston bowl mounted window using a Photron SA-Z high-speed camera connected to a Lambert high-speed HiCATT intensifier. The camera was equipped with 105 mm UV f/2.8 Nikkor lens and a 5 nm narrowband filter centered at 420 nm to isolate OH* emission. Geometric parameters of the three pre-chambers investigated are summarized in Table 1. The PCs have been designed by CMT-Motores Térmicos.

Tab. 1 Main geometrical parameters of the pre-chambers.

Tip	PC 1	PC 2	PC 3
Volume [cm^3]	2.0	1.7	1.7
Radial nozzle number	6	6	6
Radial nozzles diameter [mm]	0.8	0.8	1.2
Axial nozzle number	1	1	0
Axial nozzle diameter [mm]	1.0	1.0	-

A conventional inductive spark plug ignition system (ISP) was utilized as the baseline pre-chamber igniter. The second ignition system generated NRP plasma discharges utilizing a nanosecond DC pulse generator. The charge equivalence ratio (ϕ) was reduced by steps of 0.1 by increasing the flow rate of intake air, until the lean limit was reached with both ignition systems. Moreover, the fuel flow rate was adjusted to maintain a fixed 3.5 bar indicated gross mean effective pressure (IMEP$_g$) load for all conditions.

RESULTS AND DISCUSSION

Ensemble average main chamber HRR profiles for the three PC geometries and the two ignition systems are plotted for the highest (0.94) and lowest (0.71) ϕ value in Fig. 1. The Coefficient of Covariation (COV) is also reported in the legend for each condition. Comparing the HRR profiles at $\phi \approx 0.94$ between the different PC geometries with ISP as ignition systems, note that PC 1 and PC 2 feature a 55% higher peak HRR value and a narrower profile compared to PC 3. Whereas, when the NRP ignition system is utilized, PC 1 shows the highest peak HRR value, which is 43% and 67% higher than PC 2 and PC 3, respectively.

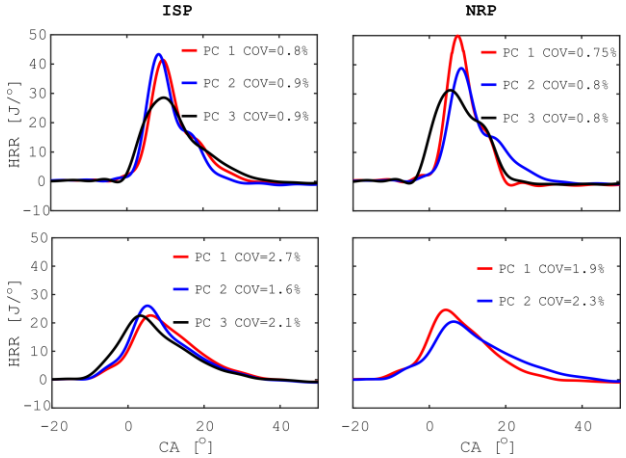

Fig. 1: Ensemble average (100-cycles) HRR for $\phi \approx 0.94$ (top row) and $\phi \approx 0.71$ (bottom row) as well as for the ISP (left) and the NRP ignition systems (right), with COV for each condition reported in the legend.

When ϕ is reduced to 0.71, the peak HRR value is similar between the PC geometries and the two ignition systems. However, PC 1 features a higher peak value and a narrower profile with the NRP ignition system as compared to the ISP. Note that ϕ values lower than 0.75 could not be reached for PC 3 with the NRP ignition system due to the presence of numerous misfires events, and thus HRR is not reported in Fig. 1 for this condition.

Heat release characteristics for the differing PC geometry and ignition systems are complemented by OH* chemiluminescence images of main-chamber combustion processes. Figure 2 compares the ignition and combustion process in the main chamber generated by the PC 1 (top row) and PC 3 (bottom row) at $\phi \approx 0.94$. Combustion images for PC 2 (not shown) have similar combustion behavior relative to PC 1. From Fig. 2 it can be observed that the combustion process generated by PC 1 is controlled by the interaction between the axial and the radial jets, while PC 3 only generates radial jets.

The combined axial and radial jets (PC 1 and PC 2) generated faster ignition due to the rapid succession of core and squish volume combustion that can be observed in the narrow bi-modal HRR peaks in Fig. 1. The larger volume PC 1 with NRP ignition system experienced faster main-chamber HRR relative to the smaller PC volume from PC 2 that resulted in overall slower combustion relative to the same condition with ISP regardless of ϕ, while no relevant differences were observed for PC 3. Additional studies will be performed to explain these trends.

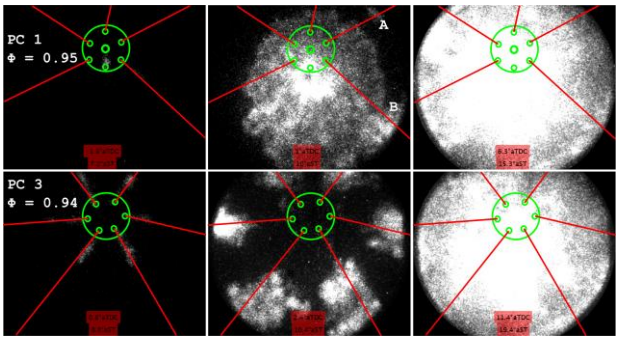

Fig. 2 OH* chemiluminescence images of the main chamber combustion for the ISP ignition system at $\phi \approx 0.95$. The image CA is reported with respect to TDC (aTDC) and the spark timing (aST). Green circles highlight the position of the pre-chamber tip and nozzles, while the red lines define the trajectory of the hot jets exiting the pre-chamber. The letters A and B highlight a specific part of the combustion process.

Additional details on the interaction between radial and axial jets for a lean condition ($\phi \approx 0.71$) are provided in Fig. 3. Note that the ignition process of PC 2 is not shown since it is very similar to PC 1. Observing the first row of Fig. 2, it is notable that the main chamber is ignited by the combination of the axial and radial jets (see points A and B). Whereas, when the equivalence ratio is decreased, the radial jets appear to be absent (see first row of Fig. 3), leaving the combustion process to rely only on the slow flame generated by the axial jet. However, when the NRP ignition system is implemented, the radial jets appear to be active again (see point C in the second row of Fig. 3). The absence of the radial jets at $\phi \approx 0.71$ led to slower ignition for PC 1 and PC 2 since the squish region ignition was delayed. As a result,

combustion progression is very similar to PC 3 as shown in Fig. 1.

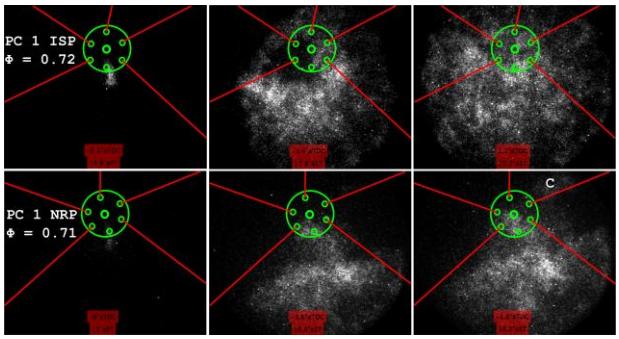

Fig. 3 OH* chemiluminescence images of the main chamber combustion for the ISP ignition system at $\phi \approx 0.71$. The image CA is reported with respect to TDC (aTDC) and the spark timing (aST). Green circles highlight the position of the pre-chamber tip and nozzles, while the red lines define the trajectory of the hot jets exiting the pre-chamber. The letter C highlights a specific part of the combustion process.

When the NRP ignition system is utilized for PC 1 (i.e., active radial jets), the HRR profile features a higher peak value and a narrower profile compare to the ISP case at $\phi \approx 0.71$, further supporting the importance of the radial jets for the overall engine performance. Additional analysis should be carried out to investigate why the radial jets are not generated at lean conditions and what parameters control the appearance of these jets.

CONCLUSIONS

Results are presented for investigations into the effects of different passive pre-chamber geometries and ignition systems on engine performance with companion flame-front imaging performed to elucidate details of combustion. Three different pre-chamber geometries were investigated along with ISP and the NRP ignition systems. The HRR profiles for the highest and lowest operating ϕ have been shown and analyzed. The main findings of this work are:

- At $\phi \approx 0.94$, the PC geometries that features radial and axial nozzles (i.e., PC 1 and PC 2) exhibit faster ignition as compared to the geometry with only radial nozzles (i.e., PC 3) due to nearly simultaneous ignition within the core of the combustion chamber and in the squish region. Ignition was further enhanced for the largest pre-chamber volume with NRP ignition (PC 1), but was slower for PC 2.
- At $\phi \approx 0.71$, all the PC geometries feature a similar combustion duration and HRR profile. This is probably due to the absence of the radial jets that strongly influences the performance of PC 1 and PC 2. The introduction of the NRP ignition system seems to keep the radial jets alive for PC 1, resulting in a faster combustion process and higher peak value of the HRR profile.
- There are clear symbiotic benefits with combinations of radial and axial nozzles and faster pre-chamber igniter systems such as the NRP. However, there are unknown variances for internal pre-chamber combustion and main-chamber jet ignition processes that remain unresolved.

REFERENCES

[1] G. J. Germane, C. G. Wood, and C. C. Hess, “Lean combustion in spark-ignited internal combustion engines-a review,” 1983.
[2] F. A. Ayala, M. D. Gerty, and J. B. Heywood, SAE Trans., pp. 177–195, 2006.
[3] L. A. Graham, S. L. Belisle, and P. Rieger, Atmos. Environ., vol. 43, no. 12, pp. 2031–2044, 2009.
[4] N. Hayashi, A. Sugiura, Y. Abe, and K. Suzuki, SAE Int. J. Engines, vol. 10, no. 3, pp. 984–994, 2017.
[5] S. Biswas, I. Ekoto, D. Singleton, K. Mixell, and P. Ford, Internal Combustion Engine Division Fall Technical Conference, 2020, vol. 84034, p. V001T03A015.
[6] W. P. Attard, M. Bassett, P. Parsons, and H. Blaxill, SAE Technical Paper, 2011.
[7] R. Novella et al., SAE Technical Paper, 2020.
[8] L. Zhou, Y. Song, J. Hua, F. Liu, Z. Liu, and H. Wei, Fuel, vol. 308, p. 121902, 2022.
[9] Y. Ju and W. Sun, Prog. Energy Combust. Sci., vol. 48, pp. 21–83, 2015.
[10] S. Biswas, I. Ekoto, and R. Scarcelli, Ignition Systems for Gasoline Engines: 4th International Conference, December 6-7, 2018, Berlin, Germany. Ed.: M. Günther, 2018, p. 311.
[11] L. Merotto, M. Balmelli, W. Vera-Tudela, and P. Soltic, Combust. Flame, vol. 237, p. 111851, 2022.
[12] S. Biswas and I. Ekoto, SAE Technical Paper, 2019.